

Thermalization in a closed quantum system from randomized dynamics

Nikolay V. Gnezdilov^{1,*} and Andrei I. Pavlov^{2,†}

¹*Department of Physics and Astronomy, Dartmouth College, Hanover, New Hampshire 03755, USA*

²*TKM, Karlsruhe Institute of Technology, 76131 Karlsruhe, Germany*

The emergence of statistical mechanics from quantum dynamics is a central problem in quantum many-body physics. Deriving observables aligned with the prediction of the canonical ensemble for a quantum system relies on the presence of a bath provided either as an external environment or as a larger part of a closed system. We demonstrate that thermal (canonical) observables for a whole closed quantum system of finite size can arise in the absence of a bath. These thermal observables stem from classical averaging over randomized unitary evolutions for a few-body system. The temperature in the canonical ensemble appears as a global constraint on the total energy of the system, determined by the choice of the initial state. From averaging randomized evolutions, we derive spin-spin correlation functions for a finite spin chain and show that they exhibit a temperature-dependent finite correlation length, in agreement with the prediction of the canonical ensemble. This establishes a method for computing thermal observables in a closed, finite-size system from real-time propagation without a bath. An implementation of this thermalization approach on a quantum computer can be utilized for thermal state preparation.

Introduction. In statistical mechanics, computing physical observables at finite temperature assumes the presence of a thermal bath – a larger environment connected to a system that sets the temperature of the canonical ensemble via energy exchange with the bath. In contrast, at the quantum mechanical level, we often consider closed systems that evolve under unitary dynamics. The process through which quantum unitary dynamics gives rise to thermal observables is known as thermalization [1–4]. In a closed quantum system that undergoes thermalization, canonical averages emerge at the subsystem’s scale, where observables are measured locally, while the rest of the system effectively acts as a bath taken in the thermodynamic limit [5–7]. In practice, numerical [8–12] and experimental [13, 14] studies indicate that for a finite-size system split into a subsystem and a bath, local observables can approach their canonical averages.

Thermalization in finite-size systems has recently become particularly relevant for quantum computation. Potential applications of quantum computation to physics and chemistry imply the ability of programmable quantum processors to simulate thermal behavior [15–18]. However, the current and near-term quantum processors operate with systems far from the thermodynamic limit. Hence, generating thermal observables for quantum few-body systems is essential. The natural thermalization process has inspired several methods for preparing thermal states on quantum hardware by engineering system-bath interactions/dissipative dynamics in a simulated system [19–28].

In this paper, we establish that observables matching those from the canonical ensemble can be obtained for a closed finite quantum system. Rather than reserving part of the system for a bath, we take a statistical approach, introducing random interactions within the system. In finite Fermi systems such as atomic nuclei, account of random residual interactions between single-particle (mean-

field) orbitals results in the average orbital occupations that, for large systems, were argued to agree with canonical ones, as if the system were in contact with a bath [29–31]. Here, by introducing random interactions within a few-body system, we justify that observables aligned with the prediction of the canonical ensemble occur from averaging unitary dynamics. Observables evolve in real time under a target Hamiltonian perturbed by random interactions in a strong perturbation regime, where the target Hamiltonian describes a few-body system whose thermal behavior we aim to probe. The evolved observables are averaged over realizations of random interactions. Implementing this approach in a few-qubit quantum simulation demonstrates that canonically distributed occupations of many-body eigenstates in the target system can be achieved in finite time [32].

For a finite spin chain used as our target system, we explain the thermalization mechanism behind our approach and compute several observables. We derive many-body occupations of the energy eigenstates in the target system and spin-spin correlation functions. Many-body correlation functions extracted from quantum dynamics are natural experimental probes of equilibration towards thermal equilibrium [33]. In our case, the same-time spatial correlation functions clearly exhibit a temperature-dependent finite correlation length. All observables computed by averaging randomized evolutions agree with the canonical predictions, where the temperature is universally determined for all observables by the choice of the initial state. This settles the approach to effectively obtain statistical mechanical observables in a closed few-body quantum system from real-time propagation.

The model. We sample randomized unitary evolutions for the target Hamiltonian H_0 , so that the state of the system evolves under the randomized Hamiltonian

$$H = H_0 + \mathcal{V}^{(j)} \quad (1)$$

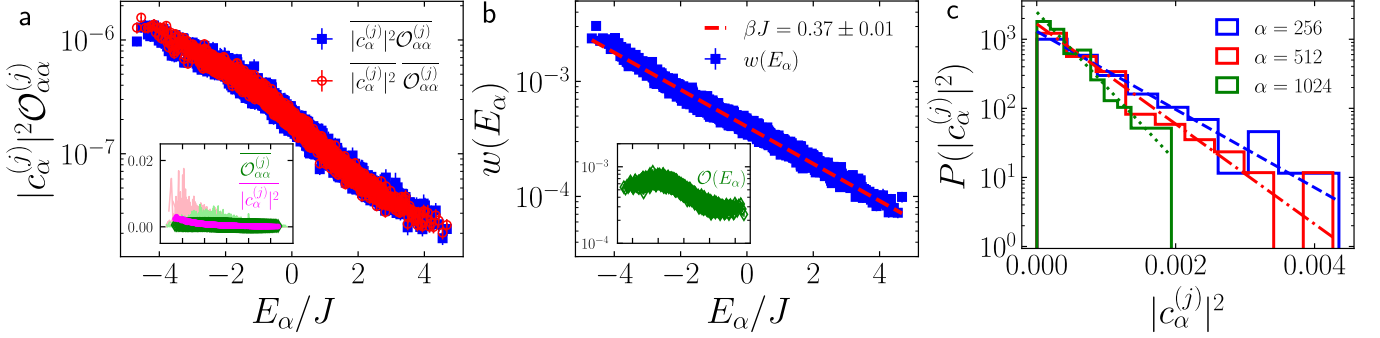


Figure 1. **Thermalization from randomized dynamics.** Panel (a) shows the eigenstate expectation value $\mathcal{O}_{\alpha\alpha}^{(j)} = \langle \psi_{\alpha}^{(j)} | \mathcal{O} | \psi_{\alpha}^{(j)} \rangle$ for $\mathcal{O} = |\varphi_{\nu}\rangle\langle\varphi_{\nu}|$ ($\nu = 500$) weighted by the eigenstate occupations in the initial state $|c_{\alpha}^{(j)}|^2 = |\langle \psi_{\alpha}^{(j)} | \psi_{\text{in}} \rangle|^2$, averaged over $M = 200$ realizations of the system versus the many-body spectrum of H . For the horizontal axis, we use the mean spectrum of H : $E_{\alpha} = \overline{E_{\alpha}^{(j)}}$. The deviations from the mean values for each energy level are small as seen from the horizontal error bars [34], defined as $\delta E_{\alpha} = \sqrt{|E_{\alpha}^{(j)} - E_{\alpha}|^2 / (M - 1)}$, which are less than the size of the marker. The blue squares display $\overline{|c_{\alpha}^{(j)}|^2 \mathcal{O}_{\alpha\alpha}^{(j)}}$ and the red circles display $\overline{|c_{\alpha}^{(j)}|^2 \mathcal{O}_{\alpha\alpha}^{(j)}}$: the two data sets lie right on top of each other. The inset shows $\overline{|c_{\alpha}^{(j)}|^2}$ and $\mathcal{O}_{\alpha\alpha}^{(j)}$. The magenta dots denote the average values $\overline{|c_{\alpha}^{(j)}|^2}$, and the pink lines display every tenth realization of $|c_{\alpha}^{(j)}|^2$ that fluctuate from realization to realization. The green diamonds and the light green lines show the same for $\mathcal{O}_{\alpha\alpha}^{(j)}$. Panel (b) shows the average eigenstate occupation probabilities $w(E_{\alpha}) = \overline{|c_{\alpha}^{(j)}|^2}$. The blue squares display $w(E_{\alpha})$, and the dashed red line corresponds to the Gibbs distribution with the temperature β^{-1} determined from Eq. (8). In the inset, the green diamonds show the average eigenstate expectation value $\mathcal{O}(E_{\alpha}) = \overline{\mathcal{O}_{\alpha\alpha}^{(j)}}$. In panels (a) and (b), the horizontal axis in the inset and in the main figure coincide. In panel (c), the blue, red, and green histograms show the probability distributions for three eigenstates of H sampled from M realizations each. The correspondingly colored lines show Porter-Thomas distribution, $P(p) = e^{-p/w(E_{\alpha})}/w(E_{\alpha})$, for each eigenstate. All figures are plotted on a log scale except for the inset in panel (a).

as $|\psi(t)\rangle = e^{-iHt}|\psi_{\text{in}}\rangle$, where $\mathcal{V}^{(j)}$ is the auxiliary random interaction between the degrees of freedom of H_0 , realizations of which correspond to different samples of time-evolution that we label by j . We choose the 1d transverse Ising model with an open boundary condition as our target Hamiltonian:

$$H_0 = -hg \sum_{i=1}^N \sigma_i^x - h \sum_{i=1}^{N-1} \sigma_i^y \sigma_{i+1}^y, \quad (2)$$

where σ_i^x and σ_i^y are the first and second Pauli matrices. We use the auxiliary interaction in the following form [32]

$$\mathcal{V}^{(j)} = - \sum_{i_1 > i_2}^N J_{i_1 i_2}^{(j)} \sigma_{i_1}^+ \prod_{k=i_2+1}^{i_1-1} \sigma_k^z \sigma_{i_2}^- + h.c.. \quad (3)$$

The coupling constants $J_{i_1 i_2}^{(j)}$ are drawn independently from the Gaussian unitary ensemble (GUE) with zero mean $\langle J_{i_1 i_2}^{(j)} \rangle = 0$ and finite variance $\langle |J_{i_1 i_2}^{(j)}|^2 \rangle = J^2/N$. We choose the initial state to be a product state ordered along σ^y : $|\psi_{\text{in}}\rangle = \otimes_{k=1}^N (i \ 1)_k^T / \sqrt{2}$, while the parameters of H_0 are $h = 0.1J$ and $g = 1.5$, which correspond to the σ^x -ordered phase of the transverse Ising model at zero temperature. We set $N = 11$ and take J as the largest energy scale in the problem. To facilitate further analysis, we define the α th eigenstate $|\psi_{\alpha}^{(j)}\rangle$ and eigenenergy $E_{\alpha}^{(j)}$ of H for its j th realization: $H|\psi_{\alpha}^{(j)}\rangle = E_{\alpha}^{(j)}|\psi_{\alpha}^{(j)}\rangle$. Simi-

larly, we introduce the ν th eigenstate $|\varphi_{\nu}\rangle$ and eigenenergy ε_{ν} of H_0 : $H_0|\varphi_{\nu}\rangle = \varepsilon_{\nu}|\varphi_{\nu}\rangle$.

Our model is ergodic, which implies that the system can achieve thermal equilibrium due to its own dynamics in the thermodynamic limit. The many-body energy spectra of ergodic systems exhibit Wigner–Dyson level statistics of random matrix theory (RMT). In the case of our model, the Hamiltonian (1) falls within the GUE class of RMT [34]. If the system obeys RMT, for $N \rightarrow \infty$, we expect that a single realization of our model will be a typical one and suffice to produce thermal observables. In what follows, we demonstrate that averaging realizations of randomized evolutions yields canonical averages for the finite-size system.

Thermalization from randomized dynamics. Let's compute the expectation value of an observable \mathcal{O} :

$$\langle \overline{\mathcal{O}} \rangle = \overline{\langle \psi(t) | \mathcal{O} | \psi(t) \rangle}, \quad (4)$$

where $\overline{\dots} = \sum_{j=1}^M \dots / M$ denotes the average over $M = 200$ realizations of the time-evolution of the state $|\psi(t)\rangle = e^{-iHt}|\psi_{\text{in}}\rangle$. We decompose the initial state in terms of the eigenstates of the total Hamiltonian (1) for every realization of the latter: $|\psi_{\text{in}}\rangle = \sum_{\alpha} c_{\alpha}^{(j)} |\psi_{\alpha}^{(j)}\rangle$. Then, we express the observable (4) as

$$\langle \overline{\mathcal{O}} \rangle = \sum_{\alpha_1 \alpha_2} \overline{c_{\alpha_1}^{(j)*} c_{\alpha_2}^{(j)} e^{i t \Delta E_{\alpha_1 \alpha_2}^{(j)} \mathcal{O}_{\alpha_1 \alpha_2}^{(j)}}} \stackrel{\text{t.av.}}{=} \sum_{\alpha} \overline{|c_{\alpha}^{(j)}|^2 \mathcal{O}_{\alpha\alpha}^{(j)}}, \quad (5)$$

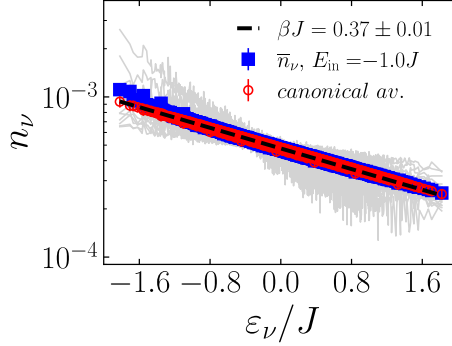


Figure 2. **Occupation probabilities of eigenstates of the Ising model** calculated by averaging randomized evolutions. The gray lines show the occupation probabilities for every tenth of the 200 realizations. The blue squares are the average occupation probabilities found from the r.h.s. of Eq. (5). The red circles are occupation probabilities found from Eqs. (7-9). The dashed black line shows occupations populated according to the Gibbs distribution with the temperature determined from Eq. (8).

where $\Delta E_{\alpha_1 \alpha_2}^{(j)} \equiv E_{\alpha_1}^{(j)} - E_{\alpha_2}^{(j)}$ and $\mathcal{O}_{\alpha_1 \alpha_2}^{(j)} \equiv \langle \psi_{\alpha_1}^{(j)} | \mathcal{O} | \psi_{\alpha_2}^{(j)} \rangle$. In the above, we performed a long-time average as a result of which, only the diagonal contributions enter the r.h.s. of Eq. (5), where $|c_{\alpha}^{(j)}|^2 = |\langle \psi_{\alpha}^{(j)} | \psi_{\text{in}} \rangle|^2$ is the occupation probability of the α th eigenstate of H (for its j th realization) in the initial state and $\mathcal{O}_{\alpha \alpha}^{(j)} = \langle \psi_{\alpha}^{(j)} | \mathcal{O} | \psi_{\alpha}^{(j)} \rangle$ is the corresponding eigenstate expectation value of the observable \mathcal{O} . For brevity, we do not introduce a separate notation for long-time averaging, but we imply it for all the observables from here on, unless stated otherwise.

So far, we have followed the standard steps that lead to thermal observables [1-3]. However, there is a crucial addition – the extra averaging over randomized realizations of H in Eq. (5), which allows us to study statistics of $|c_{\alpha}^{(j)}|^2$ and $\mathcal{O}_{\alpha \alpha}^{(j)}$ for every α . In Fig. 1a, we show that while $|c_{\alpha}^{(j)}|^2$ and $\mathcal{O}_{\alpha \alpha}^{(j)}$ may strongly fluctuate from realization to realization, their averaging over realizations can be performed independently as they are statistically uncorrelated:

$$\overline{|c_{\alpha}^{(j)}|^2 \mathcal{O}_{\alpha \alpha}^{(j)}} = \overline{|c_{\alpha}^{(j)}|^2} \overline{\mathcal{O}_{\alpha \alpha}^{(j)}}. \quad (6)$$

For the observable, we use the projector $\mathcal{O} = |\varphi_{\nu}\rangle\langle\varphi_{\nu}|$ onto the eigenstate of H_0 with $\nu = 500$. In Fig. 1a,b, we plot $\overline{|c_{\alpha}^{(j)}|^2 \mathcal{O}_{\alpha \alpha}^{(j)}}$, $\overline{|c_{\alpha}^{(j)}|^2}$, $\overline{\mathcal{O}_{\alpha \alpha}^{(j)}}$, $\overline{|c_{\alpha}^{(j)}|^2}$, and $\overline{\mathcal{O}_{\alpha \alpha}^{(j)}}$ versus the typical, i.e., mean, spectrum of H . Indeed, while the energy levels of H can change slightly from realization to realization, the deviation from the average value $E_{\alpha} = \overline{E_{\alpha}^{(j)}}$ for each energy level is small, which is justified by the size of the horizontal error bars, which is smaller than the size of the marker. Hence, we consider $\overline{|c_{\alpha}^{(j)}|^2}$ and $\overline{\mathcal{O}_{\alpha \alpha}^{(j)}}$ as functions of E_{α} : $\overline{|c_{\alpha}^{(j)}|^2} = w(E_{\alpha})$ and $\overline{\mathcal{O}_{\alpha \alpha}^{(j)}} = \mathcal{O}(E_{\alpha})$.

The average of two uncorrelated, strongly fluctuating

entities in Eq. (6) resembles the thermalization scenario #1 in Ref. [3]. In the latter scenario, the eigenstate occupations and eigenstate expectation values can exhibit strong fluctuations in a narrow energy window around the initial energy. However, these entities stay uncorrelated and average out independently in the chosen energy window. As a result, one obtains the observable consistent with the prediction of the microcanonical ensemble. The key distinction from this scenario is that, in our case, factorization of the average occurs in the domain of realizations rather than in the domain of energies.

In Fig. 1b, the average eigenstate occupations display finite overlap of the initial state with all energy eigenstates. This observation differs from conventional thermalization studies in which the broadening of the initial state in the energy space is set by the small strength of a perturbation that induces equilibration dynamics [3]. This is expected since we consider our model in the strong perturbation regime, where the characteristic energy J of the auxiliary interaction (3) is the largest energy scale in the problem, effectively extending the energy window around the initial state to the whole system. Thus, we have to account for all eigenstate expectation values $\mathcal{O}(E_{\alpha})$, each weighted by $w(E_{\alpha})$, to compute the expectation value of the observable

$$\langle \overline{\mathcal{O}} \rangle = \sum_{\alpha} w(E_{\alpha}) \mathcal{O}(E_{\alpha}), \quad (7)$$

where $\sum_{\alpha} w(E_{\alpha}) = 1$.

Since Eq. (7) includes all energy eigenstates in the system, the natural way to see thermalization at this level is to determine whether the average occupations in the initial state, $w(E_{\alpha}) = |\langle \psi_{\alpha}^{(j)} | \psi_{\text{in}} \rangle|^2$, give rise to the canonical ensemble. The corresponding temperature should be found from the total energy conservation, so that the expectation value $\langle \overline{H} \rangle = \langle \psi(t) | H | \psi(t) \rangle$ would agree with the prediction of the canonical ensemble [35]. In our case, this condition on temperature involves averaging over realizations of the system. Furthermore, for our model, the total energy is, on average, constrained by $E_{\text{in}} = \langle \psi_{\text{in}} | H_0 | \psi_{\text{in}} \rangle = \langle \overline{H} \rangle = \langle \psi_{\text{in}} | H | \psi_{\text{in}} \rangle$ due to the zero mean coupling in the auxiliary interaction (3). Combining these two conditions, the temperature in the canonical ensemble should be uniquely determined from

$$\begin{cases} \langle \overline{H} \rangle = \frac{\text{Tr}(e^{-\beta \overline{H}} \overline{H})}{\text{Tr}(e^{-\beta \overline{H}})} \\ E_{\text{in}} = \langle \overline{H} \rangle \end{cases} \Rightarrow \beta = \beta(E_{\text{in}}), \quad (8)$$

where β is the inverse temperature that explicitly depends on the choice of the initial state.

In Fig. 1b, we demonstrate that the average eigenstate occupation probabilities match the Gibbs distribution, so that

$$w(E_{\alpha}) = e^{-\beta E_{\alpha}} / \mathcal{Z}, \quad (9)$$

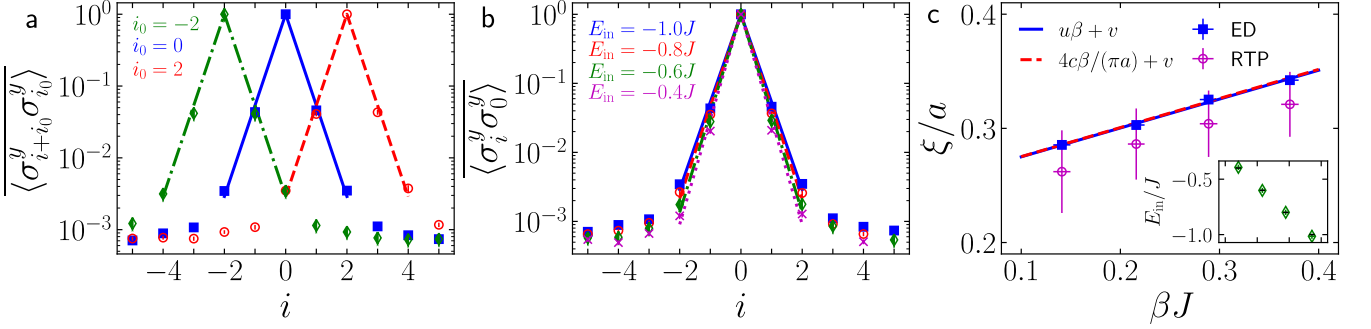


Figure 3. Correlation functions of the Ising model calculated by averaging randomized unitary dynamics. Panel (a) shows the average same-time spin-spin correlators as functions of the lattice sites on a log scale. The blue squares represent the correlator positioned at $i_0 = 0$ and the red circles and green diamonds display the correlators placed at $i_0 = 2$ and $i_0 = -2$. The correspondingly colored lines show the exponential decay with the rate determined from fitting the central correlator in the interval $i = [-2, 2]$. In panel (b), the blue squares, red circles, green diamonds, and magenta crosses show correlator positioned at $i_0 = 0$ for gradually increasing initial energies. The correspondingly colored lines show the fits performed at every initial energy E_{in} . In panel (c) we plot the coherence length ξ as a function of the inverse temperature β determined by E_{in} (with small uncertainties in the total energy $\langle \bar{H} \rangle$ that stem from averaging over realizations). The blue squares show ξ found from the fit in the central panel for the correlators computed using the exact diagonalization (ED). The magenta circles show the same for the correlators computed with the real-time propagation (RTP). The solid blue line is the linear fit for the data and the dashed red line shows predictions for ξ in the thermodynamic limit up to the finite-size offset. In the inset, the green diamonds and black dashes display $\langle \bar{H} \rangle$ and $E_{\text{in}} = \langle \psi_{\text{in}} | H_0 | \psi_{\text{in}} \rangle$ as a function of β . The horizontal axis is the same as in the main figure.

where $\mathcal{Z} = \sum_{\alpha} e^{-\beta E_{\alpha}}$ and β is determined from the condition (8). Changing the initial state accordingly changes the temperature for average eigenstate occupations [34]. The origin of the Gibbs distribution for the average eigenstate occupations $w(E_{\alpha}) = |\langle \psi_{\alpha}^{(j)} | \psi_{\text{in}} \rangle|^2$, where $|\psi_{\alpha}^{(j)}\rangle$ is the eigenstate of the Hamiltonian in the GUE class of RMT, is rooted in the properties of random quantum states of ergodic systems [36–38] that can also support global constraints [39, 40]. Within our approach, sampling many randomized realizations of the system allows us to draw the probability distribution for the eigenstate occupations $|c_{\alpha}^{(j)}|^2 = |\langle \psi_{\alpha}^{(j)} | \psi_{\text{in}} \rangle|^2$ for each individual energy eigenstate (at fixed α). In Fig. 1c, we show that this probability distribution follows the Porter-Thomas distribution [41], $P(|c_{\alpha}^{(j)}|^2) = e^{-|c_{\alpha}^{(j)}|^2/w(E_{\alpha})}/w(E_{\alpha})$, characteristic of chaotic behavior [36–38]. Subsequently, averaging realizations of each eigenstate occupation probability and plotting the mean occupations versus the mean spectrum of H leads to Fig. 1b and Eq. (9).

Observables. Calculating the expectation value of the observable requires eigenstate occupation probabilities $w(E_{\alpha}) = |\langle \psi_{\alpha}^{(j)} | \psi_{\text{in}} \rangle|^2$ and eigenstate occupation values $\mathcal{O}(E_{\alpha}) = \langle \psi_{\alpha}^{(j)} | \mathcal{O} | \psi_{\alpha}^{(j)} \rangle$. The former depend on the energy of the initial state through β and do not depend on the observable. The latter's behavior depends on the specific observable. We compute $\langle \bar{\mathcal{O}} \rangle$ for the projector $\mathcal{O} = |\varphi_{\nu}\rangle\langle\varphi_{\nu}|$ for all eigenstates $|\varphi_{\nu}\rangle$ of the Ising Hamiltonian H_0 from the r.h.s. of Eq. (5) and from Eqs. (7–9). We plot the results in Fig. 2. The occupation probabilities of the eigenstates of the Ising model computed from averaging randomized dynamics,

$\bar{n}_{\nu} = \overline{\langle \psi(t) | \mathcal{O} | \psi(t) \rangle} = \overline{|\langle \psi(t) | \varphi_{\nu} \rangle|^2}$, are thermal. The ensemble temperature is set by the energy-conservation constraint (8), and changes for different initial states [34]. For reference, we plot occupations populating the eigenstates of the Ising model according to the Gibbs distribution: $n_{\nu} = e^{-\beta \varepsilon_{\nu}} / \sum_{\nu} e^{-\beta \varepsilon_{\nu}}$. Although the Hamiltonian H_0 is integrable, adding the random interaction (3) with zero mean and large variance turns the system ergodic. Averaging randomized evolutions governed by the perturbed Hamiltonian leads to thermal observables. Choosing the observable to be the projector onto the eigenstates of H_0 results in thermal occupation of these eigenstates.

In our previous analysis, we devised the properties of the eigenstates of H to understand the mechanism behind the emergence of thermal observables. Then, we calculated the occupation probabilities of the eigenstates of the Ising model within our approach. However, both tasks require that eigenstates and eigenenergies of the system are known, which is generally not the case in quantum many-body physics. Instead, thermal behavior manifests itself in correlation functions that can be computed theoretically or measured experimentally. For the transverse-field Ising model (2), by comparing the model's parameters with the determined temperature ($\beta^{-1} \approx 2.7J \gg 2h|1-g| = 0.3J$), we expect the same-time spatial spin-spin correlation function, $\langle \sigma^y(x) \sigma^y(0) \rangle \sim e^{-|x|/\xi}$, to decay in the continuum limit with the linear-in- β coherence length $\xi = 4c\beta/\pi$ [42]. Here, $c = 2ha$ and a is the lattice constant. Having established that canonical averages can be derived for the relatively small isolated quantum system, we examine whether averaging randomized evolutions yields ther-

mal behavior in the correlation functions. To do so, we compute $\overline{\langle \sigma_{i+i_0}^y \sigma_{i_0}^y \rangle}$ using the r.h.s. of Eq. (5) for the correlation functions centered at $i_0 = -2, 0, 2$.

In Fig. 3a, the average correlation functions show a clear exponential decay over two sites on either side of their center. Then, the decay slows down and tends to saturate to a small value, which we attribute to the finite size of the system. To determine the decay rate, we fit the logarithm of the data for the centrally positioned correlator ($i_0 = 0$) by $-|x_i|/\xi$ in the interval $i = [-2, 2]$, with ξ being a fitting parameter and $x_i = ia$. We compare the spatially displaced correlators ($i_0 = -2, 2$) and the decaying function $e^{-|x_{i\pm 2}|/\xi}$, where ξ was found by fitting the central correlator. All correlation functions in the bulk of the system decay at the same rate and show good agreement with the fit. Since the initial energy determines the temperature (8), we compute the coherence length as a function of β by repeating the calculation for the central correlator for four initial states with distinct E_{in} . Increasing the initial energy leads to faster decay of the correlator, as seen in Fig. 3b. In Fig. 3c, we show that increasing the initial energy raises the temperature and suppresses the correlation length. The correlation length is linear in the inverse temperature, as expected in statistical mechanics. We fit ξ with a linear function $\xi = (u\beta + v)a$. We find an offset $\Delta\xi = va = (0.250 \pm 0.004)a$ due to the non-zero lattice spacing in the finite-size system. However, the slope $u = (0.253 \pm 0.017)J$ matches the prediction of statistical mechanics $4c/(\pi a) \approx 0.255J$ within the error bar. This highlights that computing the correlation functions for a few-body system by averaging randomized unitary dynamics yields their thermal behavior.

Using exact diagonalization to compute eigenstate occupations and expectation values, performing a long-time average, and then averaging over realizations of the auxiliary interaction in the r.h.s. of Eq. (5) is essential to explain the emergence of thermal observables in our approach. However, the approach enables deriving thermal observables directly from real-time propagation and averaging over realizations, as in Eq. (4), which does not require knowing the eigenstates of the system. Additionally, the average observables relax to the thermal equilibrium values in finite time $t \sim 1/J$ [32]. Using Eq. (4) for $Jt = 10, 20, 30, 40$, we repeat the calculation for the spin-spin correlation functions. After time-averaging the central correlator for each initial energy with the four time points, we apply the same fitting procedure as we did above to determine the coherence length. As seen in Fig. 3c, the computation recovers the temperature dependence of the coherence length derived earlier, up to a finite-size offset, within the error bar.

In this work, we use the all-to-all auxiliary interaction (3). However, we established that thermalization in our approach relies on the chaotic nature of the system's eigenstates rather than on the particular form of the interaction. Provided that the ergodic character of the

system is preserved, we expect that thermalization may be achieved when the connectivity of the auxiliary interaction is reduced. The latter is beneficial for applications of the approach to sufficiently larger systems in quantum and classical computation. In the case of reduced connectivity, the strong random perturbation will not couple all the degrees of freedom in the system instantaneously but will spread through the system in finite time, which may increase the equilibration time.

Thermalization from averaging randomized dynamics is not restricted to the observables considered above. Indeed, the chaotic behavior of individual many-body eigenstates (Fig. 1c) does not depend on the particular choice of the observable and leads to the emergence of the Gibbs distribution (9) in Eq. (7). Then, eigenstate expectation values of an arbitrary observable acquire thermal weights, allowing randomized Hamiltonian dynamics to efficiently simulate thermal behavior in a quantum few-body system beyond single-particle observables [43, 44] and deliver many-body correlation functions with characteristic temperature-dependent correlation lengths.

Discussion. We demonstrate that a statistical account of random auxiliary interactions within a closed few-body quantum system evolving in real time yields thermal (canonical) observables. Thermal observables occur without a bath introduced either as part of the system or as an external environment. Thermalization arises from the chaotic nature of individual many-body eigenstates. By sampling realizations of auxiliary interactions, we find that the occupation probability of each individual many-body eigenstate in the initial state follows the Porter-Thomas distribution. Averaging over realizations then leads to each eigenstate expectation value of the observable in Eq. (7) being weighted by the Gibbs distribution function (9). As a result, average observables, including many-body correlation functions, agree with their canonical averages even for a finite-size system. The temperature of the canonical ensemble is universally determined by a global constraint on the total energy conservation imposed by the initial state (8). In this way, to obtain thermal observables for the target system, we microscopically sample chaotic eigenstates respecting global constraints. Such sampling creates the possibility of generating random circuits that implement constrained Haar-random evolutions [39, 40] from quantum few-body Hamiltonian dynamics. In our approach, thermal equilibrium values of the observables can be obtained from real-time propagation in finite time. This enables real-time evolution-based methods in quantum simulation [32] and classical numerical computation (such as the time-dependent variational principle with matrix product states [45, 46]) to produce canonical averages in a closed quantum system without allocating a part of the system for a bath.

Acknowledgment. We thank Vanja Dunjko, Archana Kamal, Maxim Olshanii, and Thibault Scoquart

for stimulating discussions. N.V.G. thanks Alexander Shnirman for the hospitality during the visit to KIT. N.V.G. was supported by the Department of Physics and Astronomy, Dartmouth College. A.I.P. was supported by the German Ministry of Education and Research (BMBF) within the project QSolid (FKZ: 13N16151) and by the DFG Grant SH 81/8-1.

Data availability. The numerical data produced in this study are available in an open repository [47].

APPENDIX

Level statistics

Our model (1) consists of the target (2) and auxiliary (3) terms, where each of them is integrable, while their combination is not. The target system is the 1d transverse-field Ising model, and the auxiliary interaction can be mapped onto the random-hopping model using the Jordan-Wigner transform: $\mathcal{V}^{(j)} = \sum_{i_1 > i_2}^N J_{i_1 i_2}^{(j)} c_{i_1}^\dagger c_{i_2} + h.c.$, where c_i^\dagger and c_i are fermionic creation and annihilation operators at the i th site. If considered independently, the target and the auxiliary terms can be represented in terms of free fermions. To avoid integrability, we specifically choose the nearest neighbour interaction in the target system along σ^y , so that the target and auxiliary terms cannot be brought to the free-fermion form in the same basis. As a result, adding the auxiliary interaction to the target system makes the system ergodic, which we explicitly demonstrate by considering level statistics of the total Hamiltonian $H = H_0 + \mathcal{V}^{(j)}$.

The many-body energy spectra of ergodic systems follow Wigner-Dyson level statistics of random matrix theory (RMT), in contrast to those of integrable or many-body localized systems, which follow Poisson level statistics [48]. To analyze the level statistics of the total Hamiltonian (1), we use the probability distribution of a ratio $0 \leq r_\alpha^{(j)} \leq 1$ determined from two consecutive level spacings of the many-body spectrum [49]: $r_\alpha^{(j)} = \min\{\delta_{\alpha+1}^{(j)}, \delta_\alpha^{(j)}\}/\max\{\delta_{\alpha+1}^{(j)}, \delta_\alpha^{(j)}\}$, where $\delta_\alpha^{(j)} = E_{\alpha+1}^{(j)} - E_\alpha^{(j)}$. In Fig. 4, we plot the probability distribution of $r_\alpha^{(j)}$ for the 200 realizations of the Hamiltonian (1) with $N = 11$ spins, excluding two lowest and two highest energies for every realization. The resulting probability distribution in our system is consistent with the probability distribution for the GUE class of RMT, $P(r) = 2(1+r)^2/(1+r+r^2)^4/Z_2$, where Z_2 is a normalization constant. The mean value of the gap ratio \bar{r} coincides with the prediction of GUE, $\bar{r}_{\text{GUE}} \approx 0.6$ [50]. For contrast, in Fig. 4, we add the probability distribution $P(r) = 2/(1+r)^2$ for the gap ratio of an integrable or many-body localized system [49].

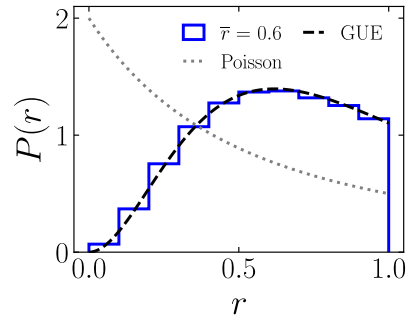


Figure 4. **Probability distribution of the ratio of consecutive level spacings.** The blue histogram shows the probability distribution of $r_\alpha^{(j)}$ sampled from the 200 realizations of the Hamiltonian H with $N = 11$. The dashed black line shows the probability distribution for a system with the level statistics described by the Gaussian unitary ensemble of random matrix theory. The dotted gray line is the probability distribution for a system with Poisson level statistics.

Different initial states

In Fig. 5, we plot average eigenstate occupations $w(E_\alpha) = |\langle \psi_\alpha^{(j)} | \psi_{\text{in}} \rangle|^2$ for several initial states with different energies. In Fig. 6, we plot occupations of the many-body eigenstates of the Ising model $n_\nu = |\langle \psi(t) | \varphi_\nu \rangle|^2$ for different initial states.

Error bars

Fig. 1. In panel (a), the vertical error bars are computed as standard errors from averaging over M realizations. The horizontal error bars are standard errors $\delta E_\alpha = \sqrt{|E_\alpha^{(j)} - E_\alpha|^2/(M-1)}$ that characterize the deviations of $E_\alpha^{(j)}$ from their mean values E_α . The error bars in panel (b) are defined in the same way.

Fig. 2. The error bars for the data displayed with the blue squares are computed as standard errors from averaging over realizations. The error bars for the data displayed with red circles are computed as $\sqrt{\mathcal{O}(E_\alpha)^2 \delta w(E_\alpha)^2 + w(E_\alpha)^2 \delta \mathcal{O}(E_\alpha)^2}$, where we use $w(E_\alpha) = e^{-\beta E_\alpha} / \mathcal{Z}$. $\delta \mathcal{O}(E_\alpha)$ are defined as standard errors from averaging $\mathcal{O}_{\alpha\alpha}^{(j)}$ over realizations. $\delta w(E_\alpha)$ are defined as $\sqrt{(\partial w(E_\alpha)/\partial \beta)^2 \delta \beta^2 + (\partial w(E_\alpha)/\partial E_\alpha)^2 \delta E_\alpha^2}$. $\delta \beta$ stems from the uncertainties δH in the total energy $\langle \bar{H} \rangle$ (calculated as standard errors from averaging over realizations) and the average thermal variance of H : $\delta \beta = \delta H / \left| \frac{\text{Tr}(e^{-\beta H} H^2)}{\text{Tr}(e^{-\beta H})} - \left[\frac{\text{Tr}(e^{-\beta H} H)}{\text{Tr}(e^{-\beta H})} \right]^2 \right|$. δE_α are the same as defined in Fig. 1.

Fig. 3. In panels (a) and (b), the vertical error bars are computed as standard errors from averaging over the realizations. In panel (c), the vertical error bars are computed as the square root of the covariance of the fit. The

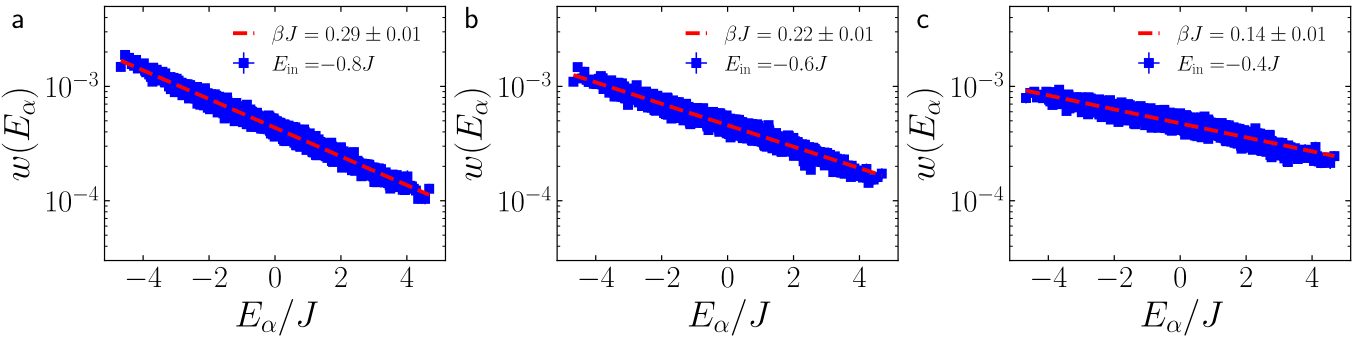


Figure 5. Average eigenstate occupation probabilities for different initial states. Legends in panels (a)–(c) are analogous to the legend in Fig. 1b.

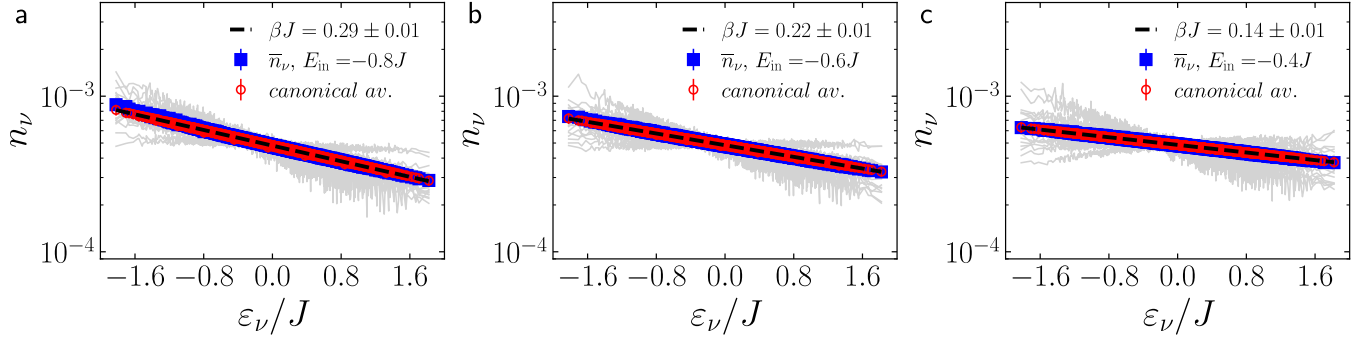


Figure 6. Occupation probabilities of eigenstates of the Ising model for different initial states. Legends in panels (a)–(c) are analogous to the legend in Fig. 2.

horizontal error bars $\delta\beta$ are the same as defined in Fig. 2. In the inset, the vertical error bars are set by δH and the horizontal error bars are the same as the vertical ones in the main figure. The length of the black dashes (E_{in}) is fixed by the error bars in β .

The error bars in Figs. 5, 6 are defined similarly to the error bars in Figs. 1b, 2, respectively.

Phys. **2**, 754 (2006).
[7] S. Goldstein, J. L. Lebowitz, R. Tumulka, and N. Zanghì, Canonical typicality, Phys. Rev. Lett. **96**, 050403 (2006).
[8] L. F. Santos, A. Polkovnikov, and M. Rigol, Weak and strong typicality in quantum systems, Phys. Rev. E **86**, 010102 (2012).
[9] S. Genway, A. F. Ho, and D. K. K. Lee, Thermalization of local observables in small Hubbard lattices, Phys. Rev. A **86**, 023609 (2012).
[10] M. Mierzejewski, T. Prosen, D. Crivelli, and P. Prelovšek, Eigenvalue statistics of reduced density matrix during driving and relaxation, Phys. Rev. Lett. **110**, 200602 (2013).
[11] J. R. Garrison and T. Grover, Does a single eigenstate encode the full Hamiltonian?, Phys. Rev. X **8**, 021026 (2018).
[12] K. Seki and S. Yunoki, Emergence of a thermal equilibrium in a subsystem of a pure ground state by quantum entanglement, Phys. Rev. Res. **2**, 043087 (2020).
[13] A. M. Kaufman, M. E. Tai, A. Lukin, M. Rispoli, R. Schittko, P. M. Preiss, and M. Greiner, Quantum thermalization through entanglement in an isolated many-body system, Science **353**, 794 (2016).
[14] F. H. B. Somhorst, R. van der Meer, M. Correa Anguita, R. Schadow, H. J. Snijders, M. de Goede, B. Kassenberg, P. Venderbosch, C. Taballione, J. P. Epping, H. H. van den Vlekkert, J. Timmerhuis, J. F. F. Bulmer, J. Lugani, I. A. Walmsley, P. W. H. Pinkse, J. Eisert, N. Walk, and J. J. Renema, Quantum simulation of thermodynamics in an integrated quantum photonic processor, Nat.

* nikolay.gnezdilov@dartmouth.edu

† andrei.pavlov@kit.edu

[1] J. M. Deutsch, Quantum statistical mechanics in a closed system, Phys. Rev. A **43**, 2046 (1991).
[2] M. Srednicki, Chaos and quantum thermalization, Phys. Rev. E **50**, 888 (1994).
[3] M. Rigol, V. Dunjko, and M. Olshanii, Thermalization and its mechanism for generic isolated quantum systems, Nature **452**, 854 (2008).
[4] L. D’Alessio, Y. Kafri, A. Polkovnikov, and M. Rigol, From quantum chaos and eigenstate thermalization to statistical mechanics and thermodynamics, Adv. Phys. **65**, 239 (2016).
[5] H. Tasaki, From quantum dynamics to the canonical distribution: General picture and a rigorous example, Phys. Rev. Lett. **80**, 1373 (1998).
[6] S. Popescu, A. J. Short, and A. Winter, Entanglement and the foundations of statistical mechanics, Nature

Commun. **14**, 3895 (2023).

[15] M. Reiher, N. Wiebe, K. M. Svore, D. Wecker, and M. Troyer, Elucidating reaction mechanisms on quantum computers, *Proc. Natl. Acad. Sci. U.S.A.* **114**, 7555 (2017).

[16] Y. Alexeev, D. Bacon, K. R. Brown, R. Calderbank, L. D. Carr, F. T. Chong, B. DeMarco, D. Englund, E. Farhi, B. Fefferman, A. V. Gorshkov, A. Houck, J. Kim, S. Kimmel, M. Lange, S. Lloyd, M. D. Lukin, D. Maslov, P. Maunz, C. Monroe, J. Preskill, M. Roetteler, M. J. Savage, and J. Thompson, Quantum computer systems for scientific discovery, *PRX Quantum* **2**, 017001 (2021).

[17] B. Faueweh, Quantum many-body simulations on digital quantum computers: State-of-the-art and future challenges, *Nat. Commun.* **15**, 2123 (2024).

[18] P. Schleich, L. B. Kristensen, J. A. C. G. Anugulo, D. Avaglano, M. Bagherimehrab, A. Aldossary, C. Gorgulla, J. Fitzsimons, and A. Aspuru-Guzik, Chemically motivated simulation problems are efficiently solvable by a quantum computer (2025), [arXiv:2401.09268 \[quant-ph\]](https://arxiv.org/abs/2401.09268).

[19] O. Shtanko and R. Movassagh, Preparing thermal states on noiseless and noisy programmable quantum processors (2023), [arXiv:2112.14688 \[quant-ph\]](https://arxiv.org/abs/2112.14688).

[20] C.-F. Chen, M. J. Kastoryano, F. G. S. L. Brandão, and A. Gilyén, Quantum thermal state preparation (2023), [arXiv:2303.18224 \[quant-ph\]](https://arxiv.org/abs/2303.18224).

[21] C.-F. Chen, M. J. Kastoryano, and A. Gilyén, An efficient and exact noncommutative quantum Gibbs sampler (2025), [arXiv:2311.09207 \[quant-ph\]](https://arxiv.org/abs/2311.09207).

[22] Z. Ding, B. Li, and L. Lin, Efficient quantum Gibbs samplers with Kubo–Martin–Schwinger detailed balance condition, *Commun. Math. Phys.* **406**, 67 (2025).

[23] D. Hahn, S. A. Parameswaran, and B. Placke, Provably efficient quantum thermal state preparation via local driving (2025), [arXiv:2505.22816 \[quant-ph\]](https://arxiv.org/abs/2505.22816).

[24] J. Lloyd and D. A. Abanin, Quantum thermal state preparation for near-term quantum processors (2025), [arXiv:2506.21318 \[quant-ph\]](https://arxiv.org/abs/2506.21318).

[25] D. Hahn, R. Sweke, A. Deshpande, and O. Shtanko, Efficient quantum Gibbs sampling with local circuits (2025), [arXiv:2506.04321 \[quant-ph\]](https://arxiv.org/abs/2506.04321).

[26] Z. Ding, Y. Zhan, J. Preskill, and L. Lin, End-to-end efficient quantum thermal and ground state preparation made simple (2025), [arXiv:2508.05703 \[quant-ph\]](https://arxiv.org/abs/2508.05703).

[27] C.-F. Chen, M. Kastoryano, F. G. S. L. Brandão, and A. Gilyén, Efficient quantum thermal simulation, *Nature* **646**, 561 (2025).

[28] H.-E. Li and L. Lin, Dissipative quantum algorithms for excited-state quantum chemistry (2025), [arXiv:2512.19870 \[quant-ph\]](https://arxiv.org/abs/2512.19870).

[29] V. Zelevinsky, B. A. Brown, N. Frazier, and M. Horoi, The nuclear shell model as a testing ground for many-body quantum chaos, *Phys. Rep.* **276**, 85 (1996).

[30] V. V. Flambaum and F. M. Izrailev, Distribution of occupation numbers in finite Fermi systems and role of interaction in chaos and thermalization, *Phys. Rev. E* **55**, R13 (1997).

[31] V. V. Flambaum and F. M. Izrailev, Statistical theory of finite Fermi systems based on the structure of chaotic eigenstates, *Phys. Rev. E* **56**, 5144 (1997).

[32] H. Perrin, T. Scoquart, A. I. Pavlov, and N. V. Gnezdilov, Dynamic thermalization on noisy quantum hardware, *Commun. Phys.* **8**, 95 (2025).

[33] S. Trotzky, Y.-A. Chen, A. Flesch, I. P. McCulloch, U. Schollwöck, J. Eisert, and I. Bloch, Probing the relaxation towards equilibrium in an isolated strongly correlated one-dimensional Bose gas, *Nature Phys.* **8**, 325 (2012).

[34] See the Appendix.

[35] M. Srednicki, The approach to thermal equilibrium in quantized chaotic systems, *J. Phys. A: Math. Gen.* **32**, 1163 (1999).

[36] T. A. Brody, J. Flores, J. B. French, P. A. Mello, A. Pandey, and S. S. M. Wong, Random-matrix physics: spectrum and strength fluctuations, *Rev. Mod. Phys.* **53**, 385 (1981).

[37] A. Mirlin, Statistics of energy levels and eigenfunctions in disordered systems, *Phys. Rep.* **326**, 259 (2000).

[38] S. Boixo, S. V. Isakov, V. N. Smelyanskiy, R. Babbush, N. Ding, Z. Jiang, M. J. Bremner, J. M. Martinis, and H. Neven, Characterizing quantum supremacy in near-term devices, *Nature Phys.* **14**, 595 (2018).

[39] D. K. Mark, F. Surace, A. Elben, A. L. Shaw, J. Choi, G. Refael, M. Endres, and S. Choi, Maximum entropy principle in deep thermalization and in Hilbert-space ergodicity, *Phys. Rev. X* **14**, 041051 (2024).

[40] M. McGinley and T. Schuster, The Scrooge ensemble in many-body quantum systems (2025), [arXiv:2511.17172 \[quant-ph\]](https://arxiv.org/abs/2511.17172).

[41] C. E. Porter and R. G. Thomas, Fluctuations of nuclear reaction widths, *Phys. Rev.* **104**, 483 (1956).

[42] S. Sachdev, *Quantum Phase Transitions* (Cambridge University Press, New York, 2011).

[43] J. D. Martin, D. Neill, A. Roggero, H. Duan, and J. Carlson, Equilibration of quantum many-body fast neutrino flavor oscillations, *Phys. Rev. D* **108**, 123010 (2023).

[44] O. Kiss, I. Tavernelli, F. Tacchino, D. Lacroix, and A. Roggero, Neutrino thermalization via randomization on a quantum processor (2025), [arXiv:2510.24841 \[quant-ph\]](https://arxiv.org/abs/2510.24841).

[45] J. Haegeman, J. I. Cirac, T. J. Osborne, I. Pižorn, H. Verschelde, and F. Verstraete, Time-dependent variational principle for quantum lattices, *Phys. Rev. Lett.* **107**, 070601 (2011).

[46] J. Haegeman, C. Lubich, I. Oseledets, B. Vandereycken, and F. Verstraete, Unifying time evolution and optimization with matrix product states, *Phys. Rev. B* **94**, 165116 (2016).

[47] Zenodo open repository, [doi:10.5281/zenodo.18021796](https://doi.org/10.5281/zenodo.18021796) (2025).

[48] M. Berry and M. Tabor, Level clustering in the regular spectrum, *Proc. R. Soc. A.* **356**, 375 (1977).

[49] V. Oganesyan and D. A. Huse, Localization of interacting fermions at high temperature, *Phys. Rev. B* **75**, 155111 (2007).

[50] Y. Y. Atas, E. Bogomolny, O. Giraud, and G. Roux, Distribution of the ratio of consecutive level spacings in random matrix ensembles, *Phys. Rev. Lett.* **110**, 084101 (2013).